Chin. J. Geochem. (2015) 34(4):515–524
DOI 10.1007/s11631-015-0069-z

ORIGINAL ARTICLE

# Geochemical characteristics of Carboniferous volcanic rocks from the Wulungu-Luliang area, Junggar basin: constraints on magma source and tectonic setting

**Wei Liu[1] · Kuihua Zhang[2] · Guanlong Zhang[2] · Peiming Zhou[1] · Qizhi Wang[1]**

Received: 2 June 2015 / Revised: 23 July 2015 / Accepted: 13 August 2015 / Published online: 30 August 2015


**Abstract** The Carboniferous volcanic rocks in the Wulungu-Luliang area are mainly andesites of medium- to high-K calc-alkalic series. Volcanic rock samples have relatively high alkali ($Na_2O + K_2O = 4.7$ % to 6.8 %) and low $TiO_2$ contents (0.7 % to 0.9 %), relatively high MgO (2.5 % to 3.4 %) and $Mg^{\#}$ (49.9 % to 67.1 %), high rare earth element (REE) contents, and relatively high $K_2O$ contents (1.7 % to 3.1 %). Chondrite-normalized REE patterns show light REE enrichment ($(La/Yb)_N = 4.15$ to 5.19) with weak Eu anomalies ($\delta Eu = 0.75$ to 0.92). These samples are enriched in large-ion lithophile elements but relatively depleted in high field strength elements. The trace elements and REE patterns are similar to those of Setouchi and central Ryukyu high-Mg andesites, indicating a high-Mg andesite source. Relatively high Y contents (16.7 to 24.4 ppm), and relatively low Sr/Y ratios (17.2 to 38.8) and $TiO_2$ contents (0.7 % to 0.9 %) exclude the possibility of slab melting. Low Sr/Nd (16.6 to 42.8), Ba/Th (66.4 to 266.8), and U/Th (0.2 to 0.3) indicate that the influence of slab-derived fluids is low. The ratios of Ce/Th (4.9–7.3), Ce/Pb (1.8–4.2), Ba/Rb (7.99–22.03), Ba/Th (66.4–266.8), and La/Sm (3.6–4.3) are similar to ratios found in subducting sediment melts. Relatively high ratios of K/Nb (1357–3258), Th/La (0.28–0.42), Zr/Nb (8.8–27.1), and especially Th/Nb (0.48–1.25) suggest that the magma was assimilated and contaminated by upper continental crust. These characteristics, along with the ratios of La/Yb, Sc/Ni, Th/Yb, Ta/Yb, $Ce/P_2O_5$, and $Zr/TiO_2$, demonstrate that the earlier Carboniferous volcanic rocks in the Wulungu-Luliang area were generated in a continental island-arc setting.

**Keywords** Junggar basin · Wulungu-Luliang area · Carboniferous · Volcanic rocks · Geochemistry · Tectonic settings

## 1 Introduction

The Wulungu-Luliang area is in the northeast of the Junggar basin, in the Qinggelidi Mountain and Luliang anteclise belt. The northern border is the Zhaheba-Beita Mountain Ophiolite belt and the southern is the Kalameili Ophiolite Belt. The Wulungu-Luliang area is a key part of the Central Asian Accretionary Orogeny and experienced multiple evolutions with different characteristics over a long geologic time. In recent years, a lot of attention, both within and outside of China, has been paid to geochemistry and tectonic settings in the Wulungu-Luliang area.

(1) The Karamaili and Zhaheba-Beita Mountain Ophiolite Belts were formed in the Paleozoic. In the mountain of Arman, the Ophiolite of Zhaheba-Beita Mountain is unconformably covered by Upper Devonian continental or transitional facies volcanic-sedimentary rock series (Li 1995).
The early Paleozoic intrusive rocks of the Artay Orogenic Belt, of which the SHRIMP age of pre-collision sequence rock is 450–467 Ma and the SHRIMP age of post-collision sequence rock is

✉ Wei Liu
littleflymn@126.com; littleflymn@126.com.cn

[1] School of Resources and Geosciences, China University of Mining and Technology, Xuzhou 221116, Jiangsu Province, People's Republic of China

[2] The West Research Center, Company of Sinopec Shengli Oilfield, Dongying 257002, Shandong Province, People's Republic of China

390–415 Ma, indicate that the collisional event represented by the Zhaheba-Beita Mountain Ophiolite occurred in the Late Cambrian–Early Ordovician and ended in the Early Devonian collisional orogenesis (Dong et al. 2012).

The Karamaili Ophiolite Belt, in which the zircon U–Pb age of gabbro is 329.9 ± 1.6 Ma (Wang 2009) and the zircon U–Pb age of plagiogranite is 373 Ma (Tang et al. 2007), shows that the Karamaili Ophiolite was formed in the Visean stage of the Early Carboniferous. There is an unconformable contact between the Ophiolite rock set and the Jiangbasitao Formation. The zircon U–Pb age of the trachyte in the Jiangbasitao Formation is 319.8 ± 2 Ma. In the late Early-Carboniferous, the Karameili area was in an intra-continental post-collision extension stage.

(2) The age of volcanic rocks around the Wulungu-Luliang area is similar to that of the Kalameili Ophiolite. The U–Pb age of volcanic rocks in the Ludong area is 321–369 Ma, dating them in the Early Carboniferous (Luo et al. 2012). The U–Pb age of the Bashan Formation volcanic rocks from the Dinan Uplift is 337.2 Ma (Li et al. 2012a, b). The zircon U–Pb age of volcanic rocks in the Sanhutang area is from 328.9 ± 1.9 to 331.3 ± 2.3 Ma. These data demonstrate that Carboniferous volcanic rocks around the Wulungu-Luliang area are related to the subduction of the Karamaili suture zone in the Early Carboniferous.

(3) The tectonic setting around the Wulungu-Luliang area is a research hotspot. I-type granites are found in the intrusive rocks of the Early Carboniferous in west Junggar, indicating a subduction event. However, the intrusive rocks of the Late Carboniferous–Early Permian are made of A-type granite, Charnockite, adakite, and high-Mg diorite, which indicate a high-temperature, extensional environment (Yin et al. 2013). Acid intrusive rocks of the Sawuer region indicate a post-collisional setting in the Early Carboniferous (Fan et al. 2007). Volcanic rocks of the Late Devonian–Early Carboniferous in Wucaiwan, Kalameili area, east Junggar formed under a post-collisional and extensional setting (Wang et al. 2014). The volcanic Batamayineishan Formation of the Ludong-Wucaiwan region formed under a post-collisional, extensional setting (Wu et al. 2009). Kalameili potassic volcanic rocks in the Batamayineishan Formation were also generated in a post-collisional setting (Yang et al. 2010). The Santanghu Basin was under a subduction-related tectonic setting in the Early Carboniferous, and entered an extensional stage after collision in the Early Carboniferous (Hao et al. 2006; Zhao et al. 2006; Li et al. 2012a, b).

The Central Asian Orogenic Belt formed in the Carboniferous in the Junggar area is characterized by obvious inhomogeneity (Gu et al. 2001). Subduction was ongoing in the Late Carboniferous in the west Junggar basin (Geng et al. 2009, 2011). There is little published geochemical data on volcanic rocks of the Carboniferous in the Wulungu-Luliang area, and no consensus has been reached about the region's Carboniferous tectonic setting. The geochemical characteristics and tectonic setting of Carboniferous volcanic rocks in the Wulungu-Luliang area are discussed herein and may prove significant in guiding the oil and gas exploration of this area in the future.

## 2 Geological settings

The Wulungu-Luliang area, located in the northeast of the Junggar basin, is a closed depression, separated from the front of Mountain Kalameili in the east by the Wulungu east fault zone, from Denan and Shiyingtan uplift in the west by the Wulanlinge fault, from the Qinggelidi Mountain piedmont zone in the north by the Tuzituoyila fault zone, and from the Luliang uplift belt in the south by the Luliang-Sangequan fault.

The Luliang Uplift belt is a typical fault-uplift belt in the north-central area of the Junggar basin, bordered by the Wulungu depression in the north, the central depression in the south, and the Kalameili suture zone in the southeast (Fig. 1). The Luliang Uplift belt is 100 km wide and extends for 200 km from northwest to southeast, covering $1.8 \times 10^4$ km$^2$.

The Luliang-Sangequan fault is in the extended line of the Kalameili ophiolite zone. In the Late Devonian–Early Carboniferous, the Kalameili remnant ocean developed

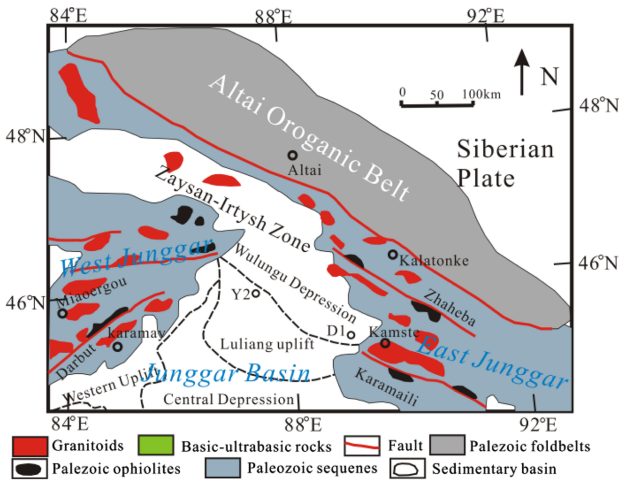


**Fig. 1** Location of Wulungu-Luliang area in the Junggar basin and the distribution of tectonic units and drilling wells

between the Wulungu Depression and the Luliang Uplift, with the Altay Archicontinent to the north and the Changji Archicontinent to the south. In the Early Carboniferous, the Kalameili remnant ocean subducted towards north and south concurrently. The Kalameili remnant ocean closed in the early part of the Late Carboniferous-Permian.

## 3 Samples and analytical method

### 3.1 Samples

The samples of this study were taken from two drilling wells in the Wulungu-Luliang area (Fig. 1). Andesite samples from Well Y2 are 319 ± 11 Ma (from Shengli Oilfield), placing the rocks in the Lower Carboniferous; volcanic rock samples from the Lower Carboniferous Jiangbasitao Formation in Well D1 are 329.3 ± 3.9 Ma, both according to zircon U–Pb SHRIMP dating (Mao 2012).

Samples from Well Y2 are mainly hornblende andesites with intertexture structure. Phenocrysts are hornblende and biotite. The matrix is dominantly plagioclase. The sizes of phenocrysts and matrix are 0.5 mm and 0.05 mm, respectively. Samples from Well D1 are andesite lithic tuff which dominantly consists of andesite lithic fragments, detrital plagioclase, and detrital quartz and tuff. The lithic fragments are about 0.2–0.5 mm with a subangular-subrounded shape. The detritus is about 0.05–0.2 mm with an angular-subangular shape.

### 3.2 Analytical method

Major elements and some trace elements (such as Sc, V, Cr, Co, Cu, Ga, S, Sr, Hf, Pb, and Th) were measured by wavelength-dispersive X-ray fluorescence spectrometry (XRF) using a BRUKER S8 TIGER spectrometer at China University of Mining and Technology. The accuracies of the XRF analyses are estimated to be about 1 % (relative) for $SiO_2$, 2 % (relative) for other major oxides presented in concentrations greater than 0.5 wt%, 5 % (relative) for minor oxides presented in concentrations between 0.1 and 0.5 wt%, and less than about 3 % for trace elements (Table 1).

Rare earth elements and U, Cs, Ta, and Y were determined by inductively coupled plasma mass spectrometry (ICP-MS)-nebulized solution method using an X Series 2 ICP-MS at the Lab of Hebei Regional Geology and Mineral Resources Researching Institution. The accuracies of the ICP-MS analyses are estimated to be better than 5 % (relative) for most elements. FeO was measured by titrimetric method at the Lab of Hebei Regional Geology and Mineral Resources Researching Institution.

## 4 Results

### 4.1 Major elements

Major element analysis results showed $SiO_2$ contents ranging from 56.8 % to 63.3 %, with an average of 59.4 %, which is mainly andesite; $K_2O$ content from 1.7 % to 3.1 %, with an average of 2.4 %; and a highly variable $K_2O/Na_2O$ ratio, from 0.39 to 1.01, with an average of 0.7 (Fig. 2). The variation probably has something to do with the alteration of the samples. Projection on a $SiO_2$ versus $Zr/TiO_2 \times 0.0001$ diagram categorized the samples as sub-alkaline area intermediate rock (Fig. 3). Among 10 samples, five plotted as high-potassium calc-alkaline rock, five as potassium calc-alkaline rock. $Fe_2O_3$ content ranged from 5.4 % to 7.2 %, with an average of 6.3 %; MgO 2.5 % to 3.4 %, with an average of 2.8 %; CaO 1.7 % to 5.3 %, with an average of 3.9 %; $Al_2O_3$ 14.1 % to 16.2 %, with an average of 15.4 %; and $TiO_2$ 0.7 % to 0.8 %, with an average of 0.8 %. $TiO_2$ content of all samples was less than 1.2 %, which is markedly different from oceanic island basalt ($TiO_2 > 2.0$ %) and MORB volcanic rock ($TiO_2$ average of 1.5 %), but similar to island arc volcanic rocks ($TiO_2$ average of 0.8 %), indicating that the rocks might have formed during the subduction process.

### 4.2 Rare earth elements and trace elements

Rare earth and trace element distribution in Carboniferous intermediate volcanic rocks are almost the same in the Wulungu-Luliang area. The range for REEs (ΣREE) was 74.3 to 120.4 ppm, averaging 103.9 ppm with high rare-earth content. The REE content distribution patterns display a right-dipping curve with strong enrichment of light REEs (LREEs), along with apparently negative Eu anomalies (δEu 0.75 to 0.93, with an average of 0.83); δCe ranged from 0.89 to 0.94, with an average of 0.92—slightly depleted. $La_N/Yb_N$ ranged from 4.15 to 5.19, with an average of 4.76, indicating relative enrichment of LREEs. $Gd_N/Yb_N$ was 1.23–1.41, with an average of 1.33, implying that fractional distillation of heavy REEs (HREEs) was not significant (Figs. 4 and 5).

In the N-MORB normalized spider diagram of Carboniferous intermediate-acid volcanic rock samples from the Wulungu-Luliang area, large-ion lithophile elements (LILEs) K, Cs, and Ba are relatively enriched; at the same time, high field strength elements (HFSEs) (including Nb, Ta, Ti, and P) are relatively depleted, and Pb is strongly enriched (Figs. 6 and 7).

## 5 Discussions

### 5.1 Source discussion

Samples of Carboniferous volcanic rocks in the Wulungu-Luliang area all showed the same or similar REE and trace

**Table 1** Major element and trace element compositions and some ratios of Carboniferous volcanic rocks from the Wulungu-Luliang area

| Sample | D1-1 VOL | D1-2 VOL | D1-3 VOL | D1-4 VOL | D1-5 VOL | Y2-1 AND | Y2-2 AND | Y2-3 AND | Y2-4 AND | Y2-5 AND |
|---|---|---|---|---|---|---|---|---|---|---|
| *Major elements (wt%)* | | | | | | | | | | |
| $SiO_2$ | 56.8 | 60.2 | 63.3 | 59.0 | 58.6 | 57.9 | 59.1 | 60.0 | 59.2 | 60.0 |
| $Al_2O_3$ | 14.7 | 15.3 | 14.1 | 15.7 | 16.2 | 16.1 | 15.8 | 15.5 | 15.4 | 15.5 |
| [a]$Fe_2O_3t$ | 6.8 | 6.4 | 5.4 | 6.9 | 7.2 | 6.1 | 6.2 | 5.8 | 5.9 | 5.9 |
| MgO | 3.4 | 3.0 | 2.5 | 2.7 | 2.6 | 2.9 | 2.8 | 2.7 | 2.6 | 2.7 |
| $Na_2O$ | 3.3 | 4.3 | 4.7 | 3.0 | 2.3 | 2.9 | 3.7 | 3.5 | 3.7 | 3.6 |
| $K_2O$ | 1.8 | 1.7 | 2.1 | 2.1 | 2.3 | 2.3 | 2.7 | 2.8 | 3.0 | 3.1 |
| CaO | 3.8 | 3.7 | 1.7 | 2.6 | 2.6 | 5.3 | 5.0 | 5.0 | 4.7 | 4.5 |
| $TiO_2$ | 0.85 | 0.70 | 0.73 | 0.83 | 0.84 | 0.78 | 0.79 | 0.78 | 0.74 | 0.75 |
| MnO | 0.14 | 0.12 | 0.09 | 0.16 | 0.17 | 0.10 | 0.11 | 0.11 | 0.11 | 0.11 |
| $P_2O_5$ | 0.17 | 0.16 | 0.16 | 0.19 | 0.19 | 0.25 | 0.28 | 0.27 | 0.27 | 0.26 |
| FeO | 4.3 | 4.0 | 2.6 | 4.3 | 4.7 | 2.6 | 2.7 | 3.0 | 3.0 | 3.2 |
| L.O.I | 8.5 | 4.7 | 5.4 | 7.1 | 7.2 | 5.1 | 3.7 | 3.8 | 0.0 | 3.7 |
| [b]$Mg^{\#}$ | 58.6 | 57.6 | 63.2 | 52.3 | 49.9 | 67.1 | 64.7 | 61.3 | 60.6 | 59.9 |
| *Trace elements (ppm)* | | | | | | | | | | |
| Sc | 21.1 | 17.0 | 15.7 | 19.0 | 19.2 | 16.8 | 15.3 | 13.7 | 13.4 | 11.9 |
| V | 144 | 140 | 140 | 146 | 148 | 137 | 135 | 126 | 125 | 120 |
| Cr | 137 | 124 | 157 | 128 | 138 | 124 | 132 | 114 | 111 | 159 |
| Ni | 25.3 | 18.1 | 55.3 | 30.7 | 35.1 | 17.5 | 15.7 | 13.8 | 11.2 | 15.5 |
| Co | 17.6 | 16.3 | 15.2 | 15.4 | 15.7 | 15.4 | 16.0 | 14.7 | 14.3 | 14.4 |
| Cu | 34.3 | 24.2 | 42.8 | 40.3 | 39.7 | 49.2 | 51.4 | 48.0 | 47.7 | 64.3 |
| Ga | 17.5 | 17.8 | 14.4 | 18.9 | 20.3 | 17.4 | 17.1 | 17.7 | 17.1 | 18.3 |
| S | 431 | 639 | 818 | 599 | 801 | 5124 | 1482 | 828 | 852 | 686 |
| Sr | 640 | 572 | 661 | 548 | 419 | 381 | 464 | 412 | 435 | 421 |
| Zr | 137 | 107 | 95 | 138 | 127 | 172 | 185 | 195 | 142 | 187 |
| Nb | 5.8 | 5.8 | 9.7 | 9.5 | 14.3 | 7.0 | 6.8 | 7.3 | 16.2 | 9.0 |
| Hf | 3.5 | 3.1 | 3.3 | 4.4 | 4.8 | 5.1 | 5.1 | 5.4 | 5.6 | 5.6 |
| Pb | 8.9 | 15.2 | 7.5 | 14.6 | 16.6 | 9.0 | 11.9 | 12.3 | 19.5 | 12.6 |
| Ba | 737 | 782 | 771 | 497 | 578 | 729 | 1091 | 1074 | 2108 | 1056 |
| Rb | 46.3 | 36.2 | 49.6 | 61.8 | 72.3 | 67.7 | 84.7 | 84.2 | 95.7 | 95.9 |
| Th | | | | 5.6 | 8.7 | 6.5 | 8.5 | 6.1 | 7.9 | 8.4 |
| U | 1.0 | 0.8 | 0.9 | 1.6 | 1.8 | 1.7 | 2.0 | 1.9 | 1.9 | 2.2 |
| B | 43.3 | 19.3 | 24.7 | 17.4 | 43.3 | 8.5 | 9.6 | 7.3 | 20.7 | 58.2 |
| Sn | 3.9 | 4.3 | 5.9 | 1.7 | 2.6 | 1.5 | 1.6 | 1.8 | 2.2 | 3.6 |
| Cs | 1.2 | 0.6 | 0.7 | 3.5 | 4.4 | 3.9 | 2.9 | 2.2 | 3.0 | 2.8 |
| Ta | 0.38 | 0.33 | 0.35 | 0.52 | 0.54 | 0.44 | 0.51 | 0.43 | 0.46 | 0.67 |
| Y | 20.1 | 16.7 | 17.0 | 24.3 | 24.4 | 20.5 | 22.3 | 21.6 | 23.8 | 22.8 |
| La | 14.2 | 13.3 | 12.6 | 20.0 | 21.9 | 18.2 | 20.4 | 19.7 | 20.7 | 20.4 |
| Ce | 30.4 | 27.5 | 26.1 | 40.8 | 45.0 | 37.7 | 42.0 | 39.3 | 44.6 | 42.6 |
| Pr | 4.2 | 3.8 | 3.6 | 5.6 | 5.9 | 5.4 | 5.8 | 5.5 | 6.2 | 5.9 |
| Nd | 18.2 | 15.9 | 15.5 | 23.3 | 24.3 | 22.9 | 24.4 | 23.3 | 26.2 | 24.8 |
| Sm | 4.0 | 3.4 | 3.4 | 5.0 | 5.1 | 4.9 | 5.2 | 4.9 | 5.6 | 5.3 |
| Eu | 1.1 | 1.0 | 1.0 | 1.3 | 1.3 | 1.2 | 1.4 | 1.3 | 1.4 | 1.3 |
| Gd | 3.8 | 3.1 | 3.1 | 4.6 | 4.6 | 4.3 | 4.6 | 4.4 | 4.9 | 4.7 |
| Tb | 0.6 | 0.5 | 0.5 | 0.8 | 0.8 | 0.7 | 0.8 | 0.7 | 0.8 | 0.8 |
| Dy | 3.8 | 3.2 | 3.3 | 4.6 | 4.6 | 4.2 | 4.5 | 4.3 | 4.8 | 4.5 |
| Ho | 0.76 | 0.65 | 0.66 | 0.92 | 0.93 | 0.82 | 0.90 | 0.85 | 0.94 | 0.90 |

**Table 1** continued

| Sample | D1-1 VOL | D1-2 VOL | D1-3 VOL | D1-4 VOL | D1-5 VOL | Y2-1 AND | Y2-2 AND | Y2-3 AND | Y2-4 AND | Y2-5 AND |
|---|---|---|---|---|---|---|---|---|---|---|
| Er | 2.1 | 1.8 | 1.9 | 2.6 | 2.6 | 2.3 | 2.5 | 2.4 | 2.7 | 2.5 |
| Yb | 2.3 | 2.0 | 2.0 | 2.8 | 2.8 | 2.5 | 2.7 | 2.6 | 3.0 | 2.8 |
| Lu | 0.50 | 0.43 | 0.46 | 0.60 | 0.62 | 0.61 | 0.69 | 0.66 | 0.70 | 0.69 |

*AND* andesit, *VOL* volcanics

[a] Total iron

[b] $Mg^{\#} = Mg^{2+}{}_{mol}/(Mg^{2+}{}_{mol} + Fe^{2+}{}_{mol})$

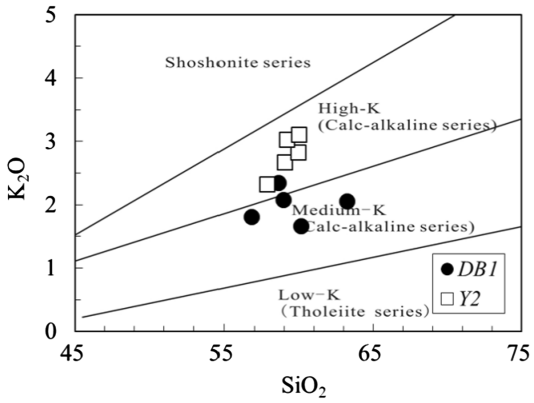


**Fig. 2** $K_2O$ versus $SiO_2$ diagrams for Carboniferous volcanic rocks from the Wulungu-Luliang area. Rock type boundaries from Rickwood (1989)

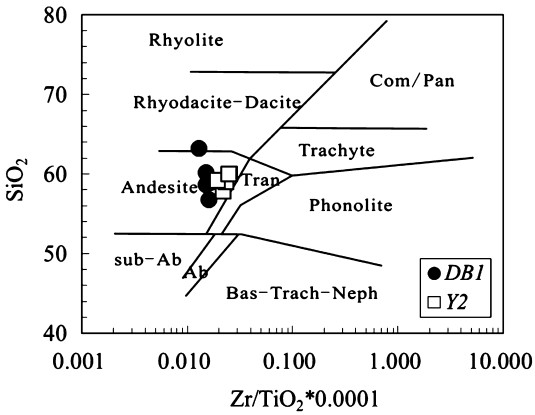


**Fig. 3** $SiO_2$ versus $Zr/TiO_2 \times 0.0001$ diagrams for Carboniferous volcanic rocks from the Wulungu-Luliang area. Rock type boundaries from Winchester and Floyd (1977)

element distribution curves. In an N-MORB normalized spider diagram, the enrichment of LILEs (K and Ba) and relative depletion of HFSEs (Nb, Ta, and Ti) may be related to oceanic crustal subduction or crustal contamination.

In an arc setting, source magma materials include: (1) peridotite in the mantle wedge; (2) fluids in subduction zones; (3) melt from the subducting slab; (4) melt from subduction sediments; and (5) assimilation and contamination of continental crust materials (Macdonald et al. 2000).

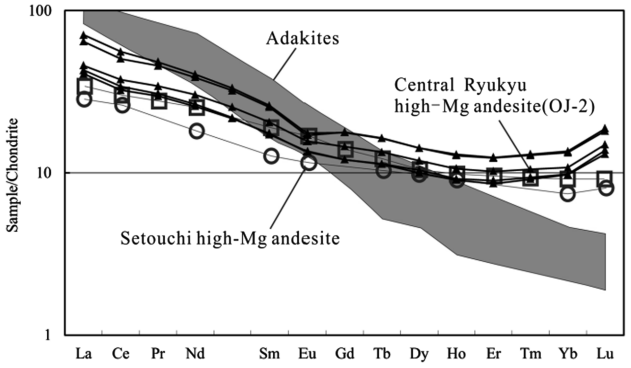


**Fig. 4** Chondrite-normalized REE patterns for Carboniferous volcanic rocks from Well D1. Normalization values from Boynton (1984). Patterns of high-Mg adakites (Kay 1978; La Yeguada—Defant et al. 1991; Cerro Pampa—Kay et al. 1993; Aleutian Adak—Yogodzinski et al. 1995; Cook Island—Stern and Kilian 1996). Patterns of high-Mg andesite (Setouchi high-Mg andesites-Shimoda et al. 1998; Central ryukyu high-Mg andesites-Shinjo 1999)

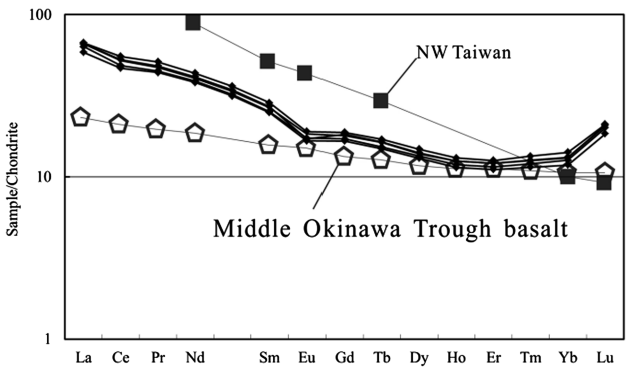


**Fig. 5** Chondrite-normalized REE patterns for Carboniferous volcanic rocks from Well Y2. Normalization values from Boynton (1984). Patterns of NW Taiwan, Middle Okinawa Trough basalts, Northern Ryukyu Volcanic front (Shinjo 1999)

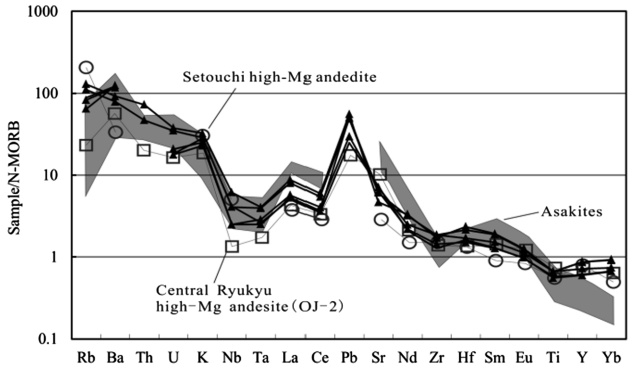


**Fig. 6** Primitive-mantle normalized spidergrams for Carboniferous volcanic rocks from Well D1. Normalized values are from Sun and McDonough (1989). Data sources are the same as in Fig. 4

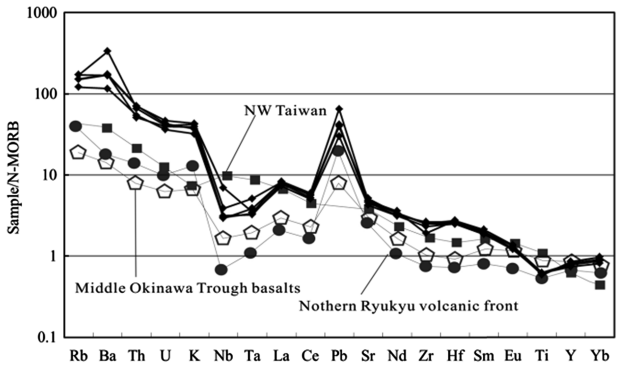


**Fig. 7** Primitive-mantle normalized spidergrams for Carboniferous volcanic rocks from Well Y2. Normalized values are from Sun and McDonough (1989). Data sources are the same as in Fig. 5

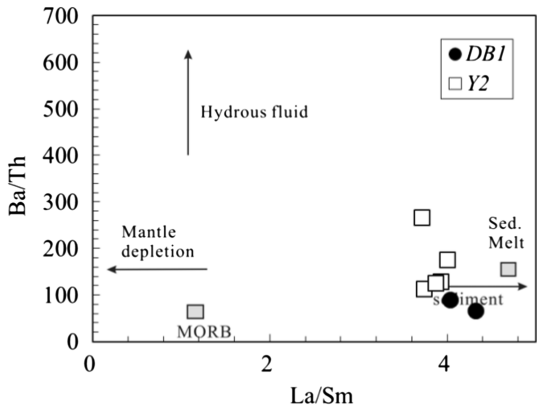


**Fig. 8** Ba/Th-La/Sm diagram for Carboniferous volcanic rocks from Wulungu-Luliang area after Stern et al. (2006)

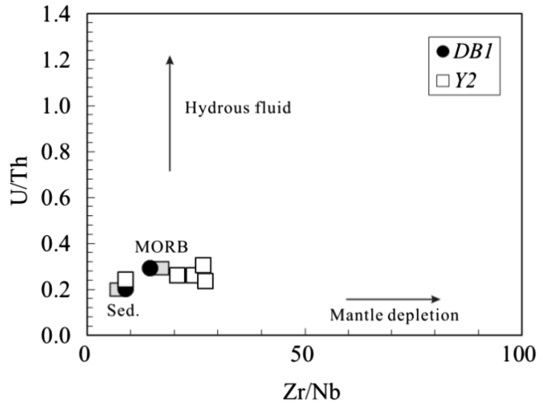


**Fig. 9** U/Th-Zr/Nb diagram for Carboniferous volcanic rocks from Wulungu-Luliang area after Stern et al. (2006)

The ratio of fluid mobile elements (like Rb, U, Ba, Sr, and Pb) to HFSEs and REEs (taken as fluid immobile elements) is an important tool to weigh the enrichment of mobile elements from the subducting slab. On the other hand, high ratios of Th/Yb and low Sr/Nd suggest the involvement of subduction sediments. In the research area, the Sr/Nd ratio of Carboniferous volcanic rocks is 16.6–42.8, with an average of 24.2; the Th/Yb ratio is 2.3–3.1, with an average of 2.8, indicating that those volcanic rocks were influenced by the involvement of subduction sediments. A high Ba/Th ratio and low La/Sm ratio are related to mantle metasomatism from fluid of subduction-induced oceanic crust metamorphism, while a low Ba/Th ratio represents the involvement of sediment melt (Stern et al. 2006). A high U/Th ratio means that the mantle source is influenced by water and fluid from the subducting slab. A high Zr/Nb ratio suggests the influence of depleted mantle. From diagrams of Ba/Th-La/Sm and U/Th-Zr/Nb (Figs. 8 and 9), it can be seen that Carboniferous volcanic rocks in the research area might have been influenced by subduction sediments, rather than fluids released from the subducting slab.

The melting of oceanic crust in the subduction process can generate adakitic magma. Overlying mantle wedge metasomated by the melt can generate adakitic rocks and high-Nb basalts. Andesite samples in the research area with Y content 16.7–24.4 and a Sr/Y ratio of 17.2–38.8 are different from those of adakite rocks (Fig. 10). Trace element distribution of the samples normalized by N-MORB also show a significant distinction between samples from the research area and standard adakitic rocks (Fig. 6).

Melt of subduction sediments is characterized by high Th and Pb content and low Ce/Th ($\approx$8), Ce/Pb ($\approx$3), Ba/Rb ($\approx$4), and Ba/Th ($\approx$111) ratios (Plank and Langmuir 1998). The Ce/Th ratio of samples in the research area was 4.9–7.3; Ce/Pb ratio was 1.8–4.2, which is far less than that of mantle (25 $\pm$ 5) and crust (<15). The Ba/Rb ratio was 8–22 and the Ba/Th ratio was 66.4–266.8. These characteristics are similar to the features of subduction sediment melt. This indicates that the magma source of the samples

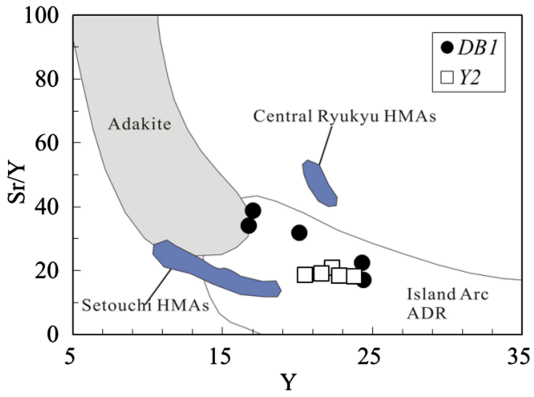


**Fig. 10** Sr/Y–Y diagram for Carboniferous volcanic rocks from Wulungu-Luliang area after Shimoda et al. (1998), data of Central ryukyu high-Mg andesites from Shinjo (1999)

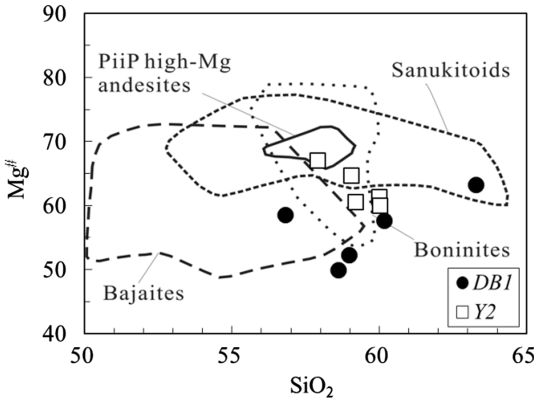


**Fig. 12** $Mg^{\#}$-$SiO_2$ diagram for Carboniferous volcanic rocks from Wulungu-Luliang area after Wang et al. (2011)

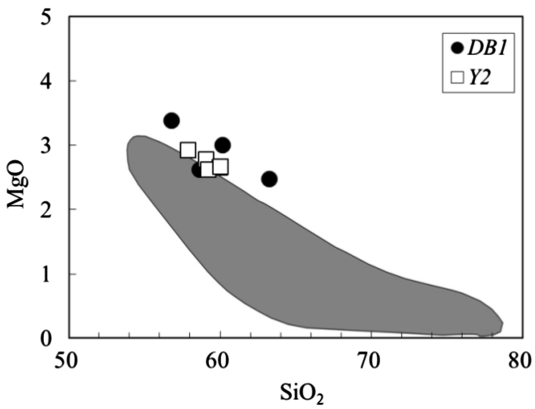


**Fig. 11** MgO-$SiO_2$ diagram for Carboniferous volcanic rocks from Wulungu-Luliang area after Martin et al. (2005); *grey field* represent chemical compositions of liquids produced by experimental melting of basalts

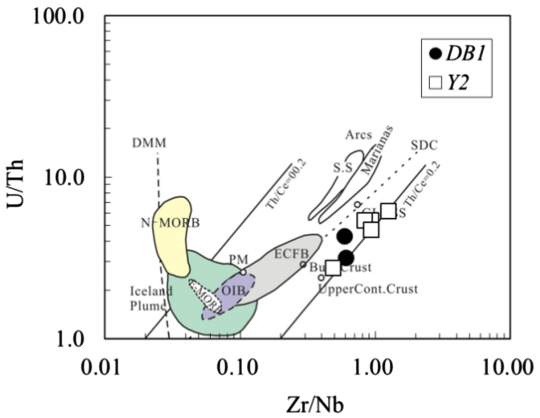


**Fig. 13** U/Th-Zr/Nb diagram for Carboniferous volcanic rocks from Wulungu-Luliang area after Song et al. (2004). *DMM* depleted mantle, *SDC* recycled subduction-derived component, *S.S* subducting sediments in arcs, *RSC* recycled residual slab comosition, *OIB* ocean-island basalt, *N-MORB* normal mid-ocean ridge basalt, *E-MORB* enriched MORB, *PM* primitive mantle

might have been influenced by the involvement of subduction sediments.

The samples analyzed are geochemically similar to high-Mg andesites from Setouchi and central Ryukyu; high-Mg andesites of Setouchi are explained by the addition of several percent of sediment melts to an inferred mantle, not by fluid addition (Shimoda et al. 1998). The samples of the research area showed relatively high Mg content compared to that of melts produced by experimental melting of basalts (Fig. 11). The high $Mg^{\#}$ is also similar to that of high-Mg andesites from Setouchi and central Ryukyu (Fig. 12). Trace element and REE patterns of our samples are overlapped on those of the Setouchi and central Ryukyu high-Mg andesites (Figs. 4, 5, 6 and 7). Sr/Y versus Y of these samples was between that of the Setouchi and central Ryukyu high-Mg andesites (Fig. 10).

Upper crust has a very high K/Nb ratio (generally more than 500) (Taylor and McLennan 1985), much higher Th/La ratio [the Th/La ratio of Primitive mantle and chondrite is about 0.12 (Sun and McDonough 1989), but continental is around 0.3 (PLANK 2005)], and higher Zr/Nb ratio (the Zr/Nb ratio of original volcanic rocks from OIB is quite low, normally 2–4, while the Zr/Nb ratio of continental crust is very high). The K/Nb ratio of Carboniferous volcanic rock samples in the research area was 1357–3258, the Th/La ratio was 0.28–0.42 (average 0.37), and the Zr/Nb ratio was 8.76–27.13 (average 18.3). K/Nb, Th/La, and Zr/Nb values suggest that the magma was contaminated by crust. In the Th/Nb-Ce/Nb diagram, Carboniferous volcanic rock samples in the research area fell on the connecting line of continental upper crust and global subduction sediments (Fig. 13). This also indicates that Carboniferous volcanic rock samples in the research area were mainly influenced by melting subduction sediment and crust contamination.

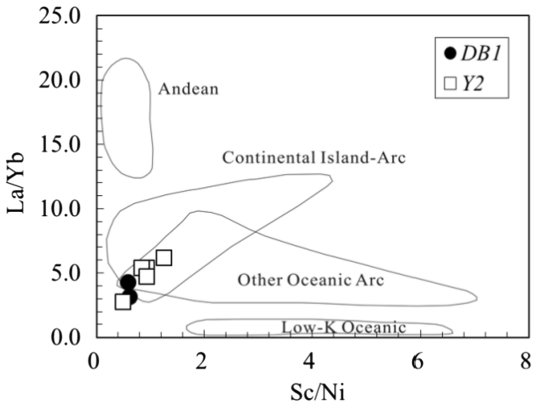


**Fig. 14** La/Yb–Sc/Ni diagram for Carboniferous volcanic rocks from Wulungu-Luliang area after Bailey (1981)

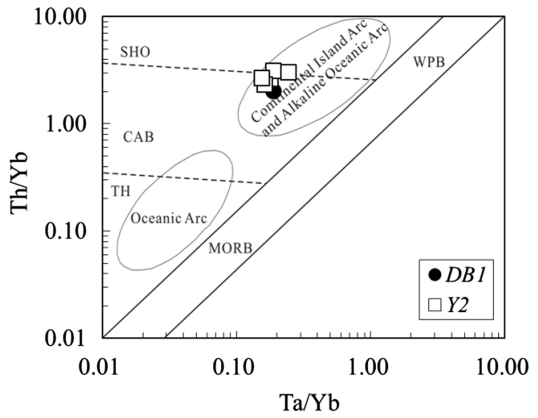


**Fig. 15** Th/Yb–Ta/Yb diagram for Carboniferous volcanic rocks from Wulungu-Luliang area after Pearce (1982)

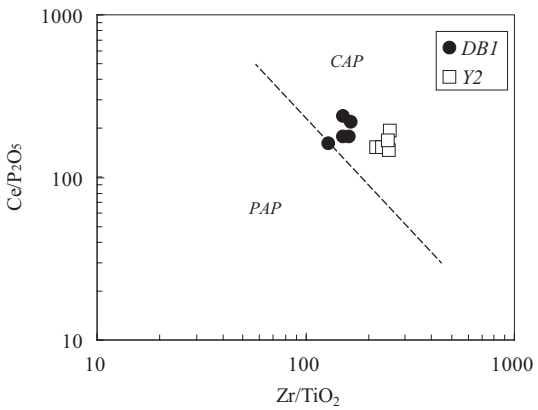


**Fig. 16** Ce/P2O5-Zr/TiO2 diagram for Carboniferous volcanic rocks from Wulungu-Luliang area after Müller et al. (1992). *CAP* Continental arc; *PAP* postcollisional arc

### 5.2 Tectonic setting

High-Mg andesite implies an arc tectonic setting. The La/Yb–Sc/Ni diagram of andesite volcanic rocks from the Wulungu-Luliang Area suggests that those samples are from an active continental-island arc (Fig. 14). In a diagram of Th/Yb–Ta/Yb, Samples of Carboniferous volcanic rocks in the research area fell into the area of continental marginal island arc (Fig. 15).

The Ryukyu arc and NW Taiwan formed in a convergent continental margin setting, which is similar to the tectonic setting of the Wulungu-Luliang area in the Carboniferous. Compared to the primitive-mantle normalized spidergrams and REE patterns of NW Taiwan, which is considered to be under post-collision conditions (Wang et al. 1999), the samples of this research were strongly depleted in Ta, Nb, and Ti and enriched in LREEs. In the Ce/P2O5–Zr/TiO2 diagram, volcanic rocks in this area plotted in the continental-island arc range, distinct from post-collisional arc (Fig. 16).

In Late Devonian–Early Carboniferous, the Kalameili remnant ocean developed between the Wulungu Depression and the Luliang Uplift. The Kalameili remnant ocean subducted toward the Altey Archicontinent in the north and the Changji Archicontinent in the south, and developed a continental-island arc and after-arc aulacogen at the Archicontinent margin (Kuang et al. 2013). In late stage of the Early Carboniferous, the Kalameili remnant ocean shrank continuously and Kalameili ocean crust sank, reducing the ocean crust subduction angle. The subducting slab rubbed against the continental edge and generated a high geothermal gradient. Subduction sediments partially melted under the high temperature and low pressure conditions, which caused the generation of high-Mg andesite melts. Those high-Mg andesite magmas were contaminated by upper crust on their way up. This subduction tectonic setting is consistent with the high-silica adakites of the Late Carboniferous in the Kalameili area (Geng et al. 2009; Geng et al. 2011). The Wulungu Depression and Luliang Uplift were in a continental-island arc tectonic setting in late stage of the Early Carboniferous and early stage of the Late Carboniferous, and were still in a subduction setting in the late stage of the Early Carboniferous.

## 6 Conclusions

The Carboniferous was a period of volcanic activity in the Junggar basin. Carboniferous volcanic rocks in the Wulungu-Luliang area are high- to medium-K calc-alkaline series intermediate volcanic rocks. Relative enrichment of

LREEs indicates that the rocks are products of primitive magma after a certain degree of differentiation. Negative Eu anomalies to some extent, flat HREE distribution, relatively enriched LILEs, depleted HFSEs (Nb, Ta, Ti, and P relatively depleted), and strongly enriched Pb support subduction zone or crust contamination.

The Mg content and $Mg^{\#}$ are relatively high. The Y content and Sr/Y ratio are between those of Setouchi and central Ryukyu high-Mg andesites. The trace element patterns and REE patterns are similar to those of Setouchi and central Ryukyu high-Mg andesites. Those characteristics indicate a high-Mg andesite source. Low ratios of Sr/Nd, Ba/Th, and U/Th show that the influence of fluid from the subducting slab is little. The ratios of Ce/Th, Ce/Pb, Ba/Rb, Ba/Th, and La/Sm are similar to those of the melt of subduction sediments. The higher ratios of K/Nb, Th/La, and Zr/Nb, and especially the ratio of Th/Nb, are similar to those of continental upper crust. Those characteristics show that the magma of Carboniferous volcanic rocks in the Wulungu-Luliang area was mainly influenced by subduction sediment melt and continental crustal contamination.

The ratios of Th/Yb, Ta/Yb, La/Yb, Sc/N, $Ce/P_2O_5$, and $Zr/TiO_2$ show that the Carboniferous volcanic rocks in the Wulungu-Luliang area are from a continental-island arc.

## References


Bailey JC (1981) Geochemical criteria for a refined tectonic discrimination of orogenic andesites. Chem Geol 32:139–154

Boynton WV (1984) Chapter 3–Cosmochemistry of the rare earth elements: meteorite studies. Developments in geochemistry 63–114

Defant MJ, Richerson PM et al (1991) Dacite genesis via both slab melting and differentiation: petrogenesis of La Yeguada volcanic complex, Panama. J Petrol 32:1101–1142

Dong LH, Qu X, Zhao TY et al (2012) Magmatic sequence of Early Palaeozoic granitic intrusions and its tectonic implications in north Altay orogen, Xinjiang. Acta Petrol Sin 28:2307–2316 **(in Chinese with English abstract)**

Fan Y, Zhou TF, Yuan F et al (2007) LA-ICP MS zircon age of Tasite pluton in Sawuer region of west Junggar, Xinjiang. Acta Petrol Sin 23:1901–1908 **(in Chinese with English abstract)**

Geng H, Sun M et al (2009) Geochemical, Sr–Nd and zircon U-Pb–Hf isotopic studies of Late Carboniferous magmatism in the West Junggar, Xinjiang: implications for ridge subduction? Chem Geol 266:364–389

Geng H, Sun M et al (2011) Geochemical and geochronological study of early Carboniferous volcanic rocks from the West Junggar: petrogenesis and tectonic implications. J Asian Earth Sci 42:854–866

Gu LX, Hu SX, Yu CS, Wu CZ, Yan ZF (2001) Initiation and evolution of the Bogda subduction torn-type rift. Acta Petrol Sin 17:585–597 **(in Chinese with English abstract)**

Hao JR, Zhou DW, Liu YQ, Xing XJ (2006) Geochemistry and tectonic settings of Permian volcanic rocks in Santanghu basin, Xinjing. Acta Petrol Sin 22:189–198 **(in Chinese with English abstract)**

Kay RW (1978) Aleutian magnesian andesites: melts from subducted Pacific Ocean crust. J Volcanol Geotherm Res 4:117–132

Kay SM, Ramos VA et al (1993) Evidence in Cerro Pampa volcanic rocks for slab-melting prior to ridge-trench collision in southern South America. J Geol 101:703–714

Kuang LC, Zhang YQ, Zha M, Chen ZH, Li L, Kong YH, Zhang Y (2013) Carboniferous tectonic setting and evolution in northern XinJiang, China. Acta Geol Sin 87:311–320 **(in Chinese with English abstract)**

Li JY (1995) Main characteristics and emplacement processes of the East Junggar ophiolites, Xinjiang, China. Acta Petrol Sin 11:73–84 **(in Chinese with English abstract)**

Li D, He DF, Tang Y, Fan C, Kong YH (2012a) Genesis of early Carboniferous volcanic rocks of the Dinan uplift in Junggar Basin: constraints to the closure time of Kalamaili Ocean. Acta Petrol Sin 28:2340–2354 **(in Chinese with English abstract)**

Li W, Liu YQ, Dong YP et al (2012b) The geochemical characteristics, geochronology and tectonic significance of the Carboniferous volcanic rocks of the Santanghu area in northeastern Xinjiang, China. Sci China Earth Sci 42:1716–1728 **(in Chinese with English abstract)**

Luo JL, Hou LH, Jiang YQ et al (2012) Chronology and tectonic settings of igneous rocks and origin of volcanic reservoirs in Ludong area, eastern Junggar Basin. Acta Petrolei Sin 33:351–360 **(in Chinese with English abstract)**

Macdonald R, Hawkesworth CJ et al (2000) The Lesser Antilles volcanic chain: a study in arc magmatism. Earth Sci Rev 49:1–76

Mao XL (2012) Research on tectonic lithofacies paleogeography and source rocks characteristics of the Carboniferous-Early Permian in the northern part of Junggar Basin.Xi'an: Northwest University (Master thesis), 1-71 (in Chinese with English abstract)

Martin H, Smithies RH et al (2005) An overview of adakite, tonalite trondhjemite granodiorite (TTG), and sanukitoid: relationships and some implications for crustal evolution. Lithos 79:1–24

Müller DGD, Rock NMS et al (1992) Geochemical discrimination between shoshonitic and potassic volcanic rocks in different tectonic settings: a pilot study. Miner Petrol 46:259–289

Pearce JA (1982) Trace element characteristics of lavas from destructive plate boundaries. Orog Andesites Relat Rocks 528–548

Plank T, Langmuir CH (1998) The chemical composition of subducting sediment and its consequences for the crust and mantle. Chem Geol 145:325–394

Plank T (2005) Constraints from thorium/lanthanum on sediment recycling at subduction zones and the evolution of the continents. J Petrol 46:921–944

Rickwood PC (1989) Boundary lines within petrologic diagrams which use oxides of major and minor elements. Lithos 22:247–263

Shimoda G, Tatsumi Y et al (1998) Setouchi high-Mg andesites revisited: geochemical evidence for melting of subducting sediments. Earth Planet Sci Lett 160:479–492

Shinjo R (1999) Geochemistry of high Mg andesites and the tectonic evolution of the Okinawa Trough-Ryukyu arc system. Chem Geol 157:69–88

Song X, Zhou M, Cao Z, Robinson PT (2004) Late Permian rifting of the South China Craton caused by the Emeishan mantle plume. J Geol Soc 161:773–781 **(in Chinese with English abstract)**

Stern CR, Kilian R (1996) Role of the subducted slab, mantle wedge and continental crust in the generation of adakites from the Andean Austral Volcanic Zone. Contrib Miner Petrol 123:263–281

Stern RJ, Kohut E et al (2006) Subduction factory processes beneath the Guguan cross-chain, Mariana Arc: no role for sediments, are serpentinites important? Contrib Miner Petrol 151:202–221

Sun SS, McDonough WF (1989) Chemical and isotopic systematics of oceanic basalts: implications for mantle composition and processes. Geol Soc Lond Spec Publ 42:313–345

Tang HF, Su YP, Liu CQ et al (2007) Zircon U-Pb age of the plagiogranite in Kalamaili belt, Northern Xinjiang and its tectonic implications. Geotecton Metallog 31:110–117 **(in Chinese with English abstract)**

Taylor SR, McLennan SM (1985) The continental crust: its composition and evolution. Blackwell Scientific Pub, Palo Alto **94**

Wang BY (2009) Study of Karamaili ophiolite complex and Jiangbasitao Volcanic Rocks in East Junggar of Xinjiang.Xi'an:Chang'an University (Master thesis) 1-58(in Chinese with English abstract)

Wang K, Chung S et al (1999) Post-collisional magmatism around northern Taiwan and its relation with opening of the Okinawa Trough. Tectonophysics 308:363–376

Wang Q, Li Z et al (2011) Late Triassic high-Mg andesite/dacite suites from northern Hohxil, North Tibet: geochronology, geochemical characteristics, petrogenetic processes and tectonic implications. Lithos 126:54–67

Wang FM, Liao QA, Fan GM et al (2014) Geological implications of unconformity between upper and middle Devonian, and 346.8 Ma post-collision volcanic rocks in Karamaili, Xinjiang. J Earth Sci 32:1243–1257 **(in Chinese with English abstract)**

Winchester JA, Floyd PA (1977) Geochemical discrimination of different magma series and their differentiation products using immobile elements. Chem Geol 20:325–343

Wu XQ, Liu DL, Wei GQ, Li J, Li ZS (2009) Geochemical characteristics and tectonic settings of Carboniferous volcanic rocks from Ludong-Wucaiwan area, Junggar basin. Acta Petrol Sin 25:55–66 **(in Chinese with English abstract)**

Yang GX, Li YJ, Tong LL et al (2010) Genesis and geochemical characteristics of the Kalamaili potassic basalt in the East Junggar, Xinjiang and tectonic implication. Acta Petrolei Sin 26:2345–2356 **(in Chinese with English abstract)**

Yin JY, Chen W, Yuan C et al (2013) Ages and tectonic implication of Late Paleozoic plutons in the West Junggar, North Xinjiang: evidence from LA-ICPMS zircon geochronology. Geochimica 42:414–429 **(in Chinese with English abstract)**

Yogodzinski GM, Kay RW et al (1995) Magnesian andesite in the western Aleutian Komandorsky region: implications for slab melting and processes in the mantle wedge. Geol Soc Am Bull 107:505–519

Zhao ZH, Guo ZJ, Han BF, Wang Y (2006) The geochemical characteristics and tectonic-magmatic implications of the latest-Paleozoic volcanic rocks from Santanghu basin, eastern Xinjiang, northwest China. Acta Petrol Sin 22:199–214 **(in Chinese with English abstract)**